# Interaction of a Starting Vortex as Well as a Vortex Street with a Traveling Shock Wave

DARSHAN S. DOSANJH* AND THOMAS M. WEEKS†
*Syracuse University, Syracuse, N. Y.*

**The passage of a shock front and the associated drift flow over a two-dimensional airfoil, at an angle of attack mounted in a shock tube, generated a columnar spiral starting vortex that interacted with the normal reflected shock. Interferometric investigations of this interaction extended considerably earlier schlieren observations by Hollingsworth and Richards. The generation of a progressive cylindrical acoustic wave front centered on the transmitted vortex and its alternate compression-rarefaction nature, as predicted by linearized analyses by Hollingsworth and Richards and later by Ribner, was experimentally verified and deviations from the predicted pressure amplitude distribution were discovered. A semiempirical relation for the wave-front pressure-amplitude distribution (expressed as a linear combination of quadrupole, dipole, and monopole acoustic sources) was found to represent closely the experimental results. The time variation of the core density of the transmitted vortex was deduced. The spiral vortex decayed essentially as a circular, incompressible viscous vortex until a neighboring high-density region appeared and the vortex decayed at a faster rate. The interaction of the reflected shock with the vortex street generated behind a circular cylinder, resulted in an abrupt change in vortex spacing and rapid dissolution of the vortex street. No well-defined acoustic wave fronts were evident behind the reflected shock front.**

## Nomenclature

| | | |
|---|---|---|
| $a$ | = | speed of sound |
| $c$ | = | airfoil chord |
| $c_l$ | = | airfoil section lift coefficient |
| $k$ | = | polytropic exponent |
| $p$ | = | static pressure |
| $p_T$ | = | threshold reference pressure |
| $P(\varphi)$ | = | pressure amplitude of acoustic pulse, $\Delta p/p_3$ |
| $r$ | = | radial distance from vortex center |
| $r_0$, $r_{0T}$ | = | incident, transmitted vortex core radius |
| $R$ | = | acoustic wave radius |
| $S$ | = | shock strength $p_2/p_1$ |
| $u_p$ | = | drift flow velocity behind incident shock front |
| $U_I$, $U_R$ | = | incident, reflected shock speed |
| $t_0$ | = | interaction time (coincidence of shock with vortex center) |
| $t$ | = | time beginning at $t_0$ |
| $\bar{t}$ | = | time beginning with initiating potential vortex |
| $w$ | = | tangential velocity within the vortex |
| $\alpha$ | = | airfoil angle of attack |
| $\gamma$ | = | specific heat ratio |
| $\Gamma_0$, $\Gamma_{0T}$ | = | incident, transmitted vortex strength |
| $\eta$ | = | nondimensional vortex radius |
| $\varphi$ | = | acoustic wave directional coordinate |
| $\rho$ | = | density |

### *Subscripts*

| | | |
|---|---|---|
| 1, 2 | = | ahead, behind incident shock front |
| 3 | = | behind reflected shock front |
| 0 | = | vortex center |
| $s$ | = | standard conditions |

## Introduction

IT is well known that sound is produced by the interaction of flow disturbances (either the vorticity, pressure, or temperature mode, or any combination of them) with shock waves. Also the interaction of any one mode of disturbance with a shock wave gives rise to all three modes of disturbance.[1, 2] The interaction of a shock wave with a velocity disturbance (i.e., turbulence or vorticity mode) has been considered by Ribner.[2] As a first step he analyzed the interaction of a plane shear wave with a shock front, which results both in refraction of the shear wave as well as in the generation of plane acoustic waves (pressure mode) in the region behind the shock front. Hollingsworth and Richards[3] attempted to demonstrate the validity of Ribner's linearized analysis of shock-shear wave interaction by experimental (schlieren) investigation of the interaction of a single columnar starting vortex with a reflected plane normal shock front in a shock tube. They observed that the interaction resulted in the generation of a single cylindrical acoustic pulse with directionally varying intensity and sign, centered on the transmitted vortex. Later they developed a heuristic analysis[4] of the interaction, in which the vortex (concentrated vorticity) was represented by a distribution of isotropic sinusoidal shear waves, thus reducing the problem to shock-shear wave interaction treated earlier by Ribner. By this analysis, Hollingsworth and Richards estimated the intensity distribution of the cylindrical acoustic wave front and predicted the wave front to be comprised of four alternate compression and expansion regions, each occupying one quadrant. Subsequently, Ribner[5] presented a more detailed analysis by actually constructing a Fourier integral of superposed shear waves to form the vortex flow. In this formulation the vortex consisted of plane sinusoidal shear waves disposed with radial symmetry. The plane sound waves produced by each shear wave-shock interaction were recombined in a Fourier integral. Ribner established that the sound waves possess an envelope that is, in fact, a growing cylindrical wave having alternate compression and rarefaction characteristics similar to the ones deduced earlier by Hollingsworth and Richards, but displaying a somewhat different form of intensity distribution. Additionally, Ribner found that the pressure amplitude diminishes as the inverse square root of the radius rather than the inverse first power of the radius as hypothesized by Hollingsworth and Richards.

Experimental examination of this analytically predicted, alternating compression-rarefaction behavior of the acoustic pulse, including quantitative measurements of the actual in-

Presented as Preprint 64-425 at the AIAA 1st Annual Meeting, Washington, D. C., June 29–July 2, 1964; revision received August 26, 1964. This research was supported by the U. S. Army Research Office-Durham: Grant DA-ARO(D)-31-124-G210.

* Professor of Mechanical and Aerospace Engineering, L. C. Smith College of Engineering. Member AIAA.

† Graduate Student, L. C. Smith College of Engineering. Student member AIAA.

tensity distribution and radial attenuation, has not been attempted until now. The interferometric and schlieren investigations of shock-vortex interaction conducted in a shock tube and described in this paper have yielded quantitative information on these points. Some interesting differences between the experimental results and the aforementioned linearized analyses have been observed. By considering a combination of quadrupole, dipole, and monopole acoustic sources within the vortex at the instant of interaction, the experimentally determined alternating compression-rarefaction nature of the sound wave has been empirically fitted.

The use of a plane normal shock front, reflected from the closed far end of the shock tube for observing the shock-vortex interaction, resulted in a transmitted vortex in essentially still air (no mean drift flow behind the reflected shock). This afforded an interesting opportunity to examine experimentally the time behavior (decay) of the flow field of a viscous spiral vortex.

In addition, some preliminary results deduced from schlieren and interferometric observations of the interaction of a Karman vortex street and a reflected plane normal shock front are reported.

## Experimental Arrangement and Procedure

The shock tube facility used in these investigations is represented schematically in Fig. 1. An NACA 23012, 1-in. chord airfoil was mounted by means of a midchord pivot pin midway between the stop and bottom walls of the shock tube. The angle of attack was variable between $-6°$ and $+12°$. A 0.25-in.-diam cylinder replaced the airfoil for the investigation of shock-vortex street interaction.

The method of generation of the starting vortex was essentially the same as that utilized by Hollingsworth and Richards,[3] i.e., it was generated by the passage of the primary (incident) shock front and the associated drift flow over the airfoil at an angle of attack. This incident shock underwent normal reflection, returning upstream to interact with the vortex (see sketch in Fig. 1). Since the vortex ahead of the reflected shock front is observed to be convected at almost the drift flow velocity (97% of it), and since there is no drift flow behind the reflected shock, the translational motion of the vortex is halted after the interaction. The vortex street and its subsequent interaction with the reflected shock was generated in much the same manner.

Initially, spark schlieren records of the vortex flow field alone, as well as the shock-vortex interaction, were obtained for a range of incident shock strengths $S = p_2/p_1$ from 1.2 to 2.0, using a 12-in. test section with top to bottom visibility. The vortex was examined at several stations between 3 and 12 chord lengths downstream from the airfoil trailing edge to determine those locations that were essentially free of the extraneous wave structure accompanying the vortex generation as well as shock reflection. This led to the design of the Mach-Zehnder interferometer test section with a number of airfoil (or circular cylinder) mounting positions located with respect to the 4-in. optical glass window (Fig. 1) such that the observed shock-vortex interaction was relatively free of extraneous waves. By keeping the airfoil angle of attack within the stall limits ($\alpha = -6°$ to $+12°$ for a chord based Reynolds number of $5 \times 10^5$), a well defined starting vortex could consistently be obtained and located to within 0.5 mm of any preselected position. Beginning at the coincidence of the shock front with the vortex center, a time consequence of interferograms of shock-vortex interaction (utilizing a magnesium spark source) were recorded over the same operating conditions covered in the schlieren investigations. It was found, however, that below $\alpha = 8°$ and/or $p_2/p_1 = 1.8$, the density change was not clearly detectable around the entire circular acoustic wavefront. Infinite as well as finite fringe interferograms were necessary to determine completely the density field, since fringe islands invariably made their

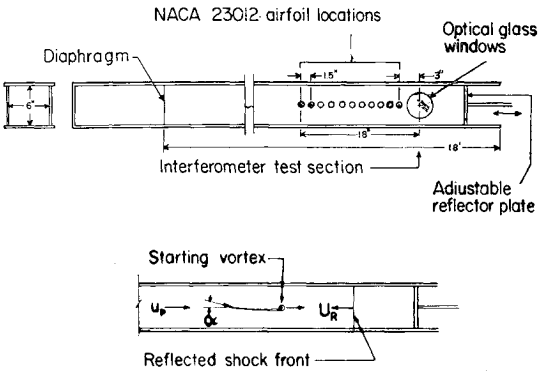


**Fig. 1 Experimental arrangement.**

appearance in the vortex core region as well as just behind the curved portion of the reflected shock front. Glass slides of interferograms were scanned using an optical comparator, and fringe position data were reduced to density profiles in numerical form utilizing an IBM 7070 computer and in graphical form with the aid of an IBM 1620 autoplotter system.

## Shock-Vortex Interaction

### Experimental Results and Discussion

The flow field produced by the passage of a plane normal shock wave over an airfoil at an angle of attack (below stall) consists essentially of the following.

1) Two diffracted, cylindrical shock waves that emanate from the leading and trailing edges of the airfoil; these waves undergo multiple reflections from the top and bottom shock tube walls as they are convected downstream with the drift flow.

2) Two pairs of slipstreams that extend from the triple intersections of the leading and trailing edge diffracted shock fronts with the receding incident normal shock front; the slipstream surfaces associated with the trailing edge diffracted shock are attached to the spiral vortex, whereas those associated with the leading edge shock front remain in close proximity to the vortex but "feed" into the airfoil wake rather than into the vortex itself.

3) The spiral vortex that appears at the instant the shock front leaves the trailing edge. For the airfoil used in these experiments, the zero lift angle of attack was $\alpha = -1.0°$, and at exactly this value, the starting vortex was observed to disappear. Further decrease in $\alpha$ resulted in an opposite sense of vortex rotation, and interactions with this vortex displayed the same characteristics as with $\alpha > -1°$ but with reversed orientation (see footnote in the section on "Comparison of Experimental Results with Earlier Analytical Predictions"). The nature of the shock induced flow, both transient and final steady state, about an airfoil is discussed in some detail by Ruetnik and Witmer.[6]

### Acoustic Wave Generation

The existence of the acoustic wave front centered on the transmitted vortex is clearly revealed in Figs. 2a–3. The horizontal knife edge (Fig. 2b) as well as corresponding vertical knife edge schlieren photographs reveal that the wave consists typically of two compression and two expansion portions distributed around the circumference. Hollingsworth and Richards did not establish experimentally the existence and/or the precise locations of these four distinct regions. Analysis of the corresponding interferograms led to the determination of the circumferential density amplitude distribution that may be converted with negligible error to pressure amplitude distribution by means of the acoustic approxima-

tion $\Delta p = a_3^2 \Delta\rho$. The distribution of pressure amplitude $P(\varphi)$ around the acoustic front corresponding to interferograms reproduced as Fig. 3 is plotted in Fig. 4. An intense compression region is found to extend from $-\varphi_{crit}$ to $\varphi = -80°$ (angles $\phi$,$\phi_{crit}$ are shown in Fig. 4). $P(\varphi)$ becomes negative in the region between $\varphi = -80°$ and $+5°$, positive between $+5°$ and $+102°$, and again negative from $+102°$ to $+\varphi_{crit}$. The decibel acoustic intensity of the compression regions may be found according to the relation $I = 20 \log \Delta p/p_T + 10 \log \rho_s a_s/\rho_3 a_3$. This yields $I = 170.8$ db corresponding to $P(-\varphi_{crit}) = 0.032$ and $I = 160.4$ db corresponding to $P(58°) = 0.023$. These experimental results are compared with the existing analytical predictions discussed below.

### Predictions by Earlier Investigators

Ribner[2] analyzed the passage of a single plane shear wave through an inclined shock front and determined that the resultant sound emission had the form of a plane sound wave inclined at the Mach angle to the refracted shear wave. Ribner pointed out that an arbitrary weak spatial distribution of vorticity could be represented as a Fourier integral of inclined plane shear waves. To verify experimentally Ribner's predictions, Hollingsworth and Richards[3] conducted a schlieren investigation of the interaction of a single columnar spiral vortex with traveling reflected plane shock front in a shock tube. They observed that the interaction results in the appearance of a cylindrical sound wave of directionally varying intensity and sign, propagating outward from the transmitted vortex. Later[4] they attempted to formulate the pressure distribution around the acoustic front utilizing Ribner's shear wave-shock interaction analysis. They did not actually formulate the Fourier integral but regarded the instantaneous perturbation velocity at a point in the vortex (assumed circular) to be equivalent to a continuous plane shear wave inclined at the same angle to the shock wave. In addition they hypothesized an $R^{-1}$ radial decay behavior of the acoustic wave front. Their result may be written in the form

$$P(\varphi) = [w_{max}/(u_p + U_R)](r_0/R)\hat{P}(\varphi) \quad (1)$$

where $\hat{P}(\varphi)$ is an interaction transfer function obtained by Ribner[2] for the individual incident shear wave.

Subsequently, Ribner[5] constructed the Fourier integral leading to a "decomposition" of a circular vortex into plane sinusoidal shear waves disposed with radial symmetry. The resulting plane sound waves were then recombined in a Fourier integral that actually demonstrated the existence of the growing cylindrical sound wave that was essentially an

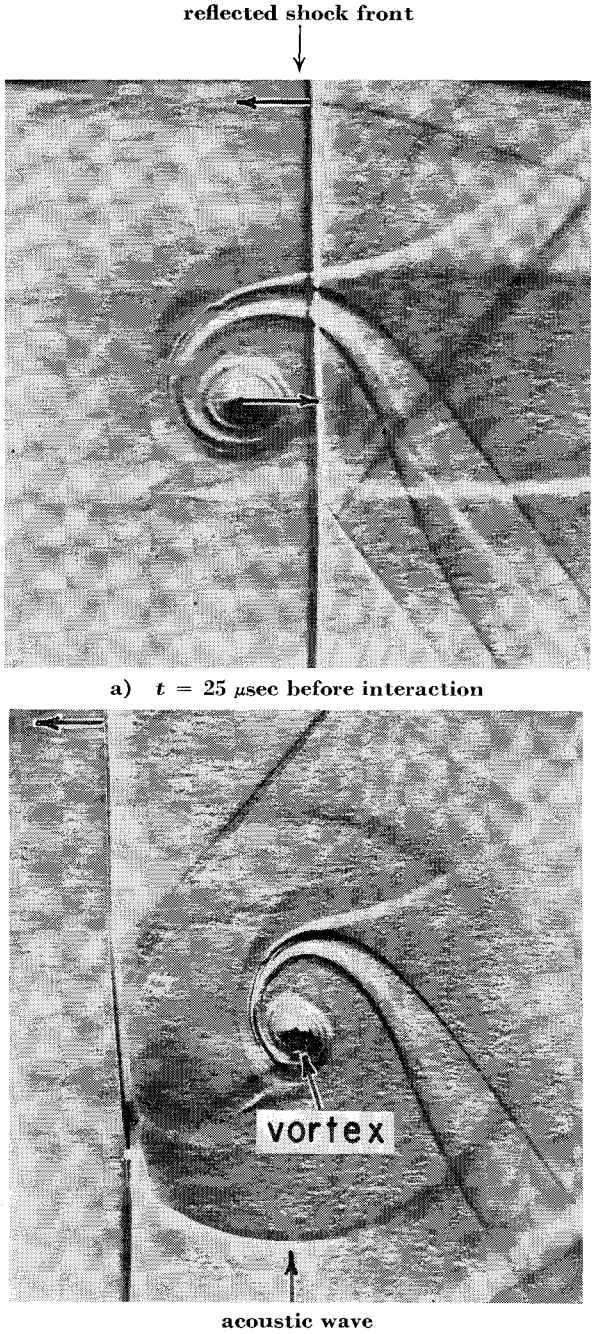


a) $t = 25$ μsec before interaction

b) $t = 80$ μsec after interaction

**Fig. 2 Shock-starting vortex interaction; horizontal knife edge schlieren $S = 1.91$ and $\alpha = 12.5°$.**

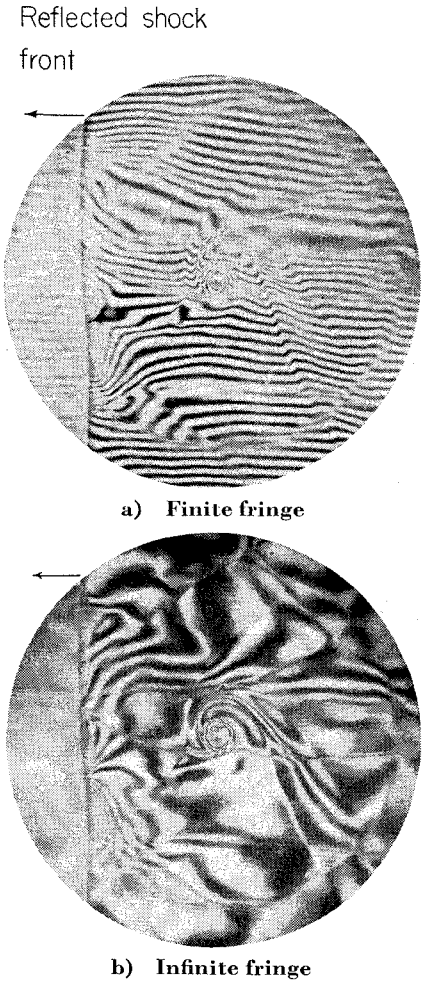


a) Finite fringe

b) Infinite fringe

**Fig. 3 Shock-starting vortex interaction; Mach Zehnder interferograms $S = 2.0$, $t = 78$ μsec, and $\alpha = 12.0°$.**

envelope of the plane sound waves. By approximate integration this led to the expression

$$P(\varphi) = \begin{Bmatrix} 2.66 \\ 1.66 \end{Bmatrix} \frac{2^{3/2}}{\pi} \frac{w_{\max}}{u_p + U_R} \left(\frac{r_{0T}}{R}\right)^{1/2} \hat{P}(\varphi) J(\varphi) \quad (2)$$

giving upper and lower bounds of the far field pressure amplitude where $J(\varphi)$ is a measure of the relative effectiveness of each plane incident shear wave in contributing to the local strength of the cylindrical sound wave at $\varphi$. The function $P(\varphi)$ corresponding to Eqs. (1) and (2) was evaluated for the operating conditions corresponding to the interferograms reproduced in Fig. 3 and compared with experimental results. In this case $u_p + U_R = 1656$ fps, $R = 0.0915$ ft. The measured core radius before interaction was $r_0 = 0.0091$ ft. The nature of the vortex after interaction will be discussed subsequently. Briefly, however, it is found to contract in the direction of shock motion into an elliptical shape with the ratio of major to minor axis given approximately by $(U_R + u_p)/U_R$, the major axis remaining equal to $2r_0$. This behavior is clearly revealed in the interaction sequence shown in Figs. 2a and 2b. It was noted that, due to shock distortion, the elliptical vortex underwent slight precession (tilting) in the direction of vortex rotation.[7] Within about 200 $\mu$sec after interaction, however, the vortex recovered its original (nearly circular) form. The core radius $r_{0T}$ of the transmitted vortex was obtained by determining the size of an equivalent circular vortex having the same core area as the actual elliptical shape. In this manner $r_{0T}$ was found to be 0.0078 ft. The maximum tangential velocity in the vortex was obtained from the relation $w_{\max} = \Gamma_0/2\pi r_0$, where $\Gamma_0$ was obtained from the Kutta-Joukowski relation that may be written as $\Gamma_0 = \frac{1}{2}(cc_l u_p)$ for unit span. The section lift coefficient $c_l$ was determined from the airfoil characteristics, corrected for Reynolds and Mach number.[8] $\Gamma_0$ was thus found to be 33.3 ft$^2$/sec and correspondingly $w_{\max} = 581$ fps. Therefore, Hollingsworth and Richards' Eq. (1) becomes

$$P(\varphi) = 0.035\hat{P}(\varphi) \quad (3)$$

in terms of Ribner's transfer function $\hat{P}(\varphi)$, whereas Ribner's result [Eq. (2)] becomes

$$P(\varphi) = \begin{Bmatrix} 0.237 \\ 0.148 \end{Bmatrix} \hat{P}(\varphi) J(\varphi) \quad (4)$$

The functions $\hat{P}(\varphi)$, $J(\varphi)$ are given in Ref. 2 for a shock Mach number $(U_R + u_p)/a_2 = 1.25$, whereas the experimental value used here was 1.29, resulting in about 1% error in $\hat{P}(\phi)$ and $J(\phi)$. Equations (3) and (4) are plotted in Fig. 4.

### Comparison of Experimental Results with Earlier Analytical Prediction

It is readily observed that Eqs. (3) and (4) and the experimental results of this investigation are similar in basic form. The circumferential distribution of pressure amplitude $P(\varphi)$ appears to be essentially quadrupole in nature. Beginning at the lower shock interception $(-\varphi_{\text{crit}})$ and proceeding in the direction of vortex rotation, first a compression region‡ is found, followed by an expansion, then a compression, and finally a second expansion region. It is apparent that the relative order of magnitude of $P(\varphi)$ for the first compression region (beginning within the order of one vortex core diameter from $-\varphi_{\text{crit}}$) is predicted well by both theoretical results. It is to be noted, however, that throughout the remainder of the acoustic wave front the agreement is only fair. It may be pointed out that, whereas the pressure distribution obtained

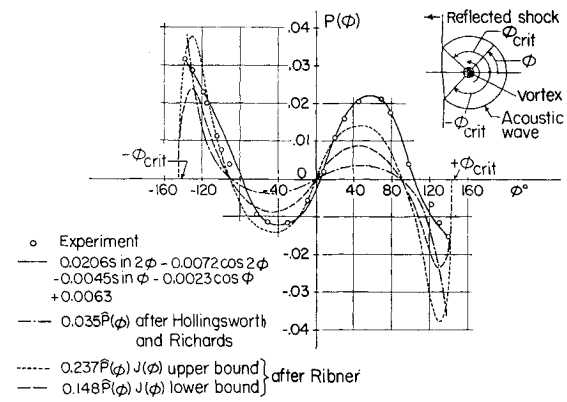


**Fig. 4 Pressure amplitude distribution around acoustic wave front (operating conditions correspond to Fig. 3).**

from linearized theory is symmetrical about $\varphi = 0$, the experimental results display definite asymmetry both in intensity and direction. Specifically, the $\varphi = 90°$, $0°$, $+90°$ reversal points predicted by both earlier theories are somewhat shifted (by different amounts) in the direction of vortex rotation. The absolute magnitudes of the pressure fluctuation at any given $\pm\varphi$ are not equal, contrary to both linearized theories. Ribner predicted $P(\pm\varphi_{\text{crit}})$ to be zero, whereas Hollingsworth and Richards predicted it to be finite by an earlier analysis in which $J(\varphi)$ (subsequently used by Ribner) was not considered. The near field effects were neglected in both analyses. Therefore, the good agreement between the experimentally observed finite values of $P(\pm\varphi_{\text{crit}})$ with those predicted by Hollingsworth and Richards may be fortuitous.

Another typical feature of shock interaction with nonuniform flow fields is distortion of the initially plane normal shock front. The shape of the shock front as well as the nature of the flow field ahead and behind are mutually (nonlinearly) dependent for finite values of upstream disturbance. These effects, not accounted for in the linearized theories by Ribner,[5] as well as by Hollingsworth and Richards,[4] do influence shock-vortex interaction phenomena.

### Semiempirical Analysis

In light of the observed differences between the experimental results and predictions of the earlier linearized analyses, an attempt was made to construct a semiempirical relationship representing the pressure amplitude distribution around the acoustic wave front. This wave front has been shown to consist of a continuous distribution of alternate compression and expansion portions, and the form of the intensity distribution appears to be essentially quadrupole in nature. The experimental pressure amplitude distribution can be represented in a Fourier series of the form

$$P(\varphi) = \frac{a_0}{2} + \sum_{n=1}^{\infty} (a_n \sin n\varphi + b_n \cos n\varphi)$$

A termwise examination reveals that the cylindrical harmonic components represent multipole acoustic sources. Existing theories[9] on aerodynamic noise generation indicate that turbulent flow fluctuations can be considered as distributions of quadrupole, dipole, and monopole acoustic sources depending on flow geometry. This involves cylindrical harmonics up to second order $(n = 2)$. Truncating the preceding series to second order yields the form

$$P(\varphi) = A \sin 2\varphi + B \cos 2\varphi + C \sin\varphi + D \cos\varphi + E \quad (5)$$

Then if the shocked vortex at the instant of interaction $(t = t_0)$ is considered as a single aerodynamic acoustic source, its radiated sound field should have the form given by Eq. (5). As a means of substantiating this, five values of $P(\varphi)$ taken at

‡ For $\alpha < 1°$, the direction of rotation of the starting vortex is reversed resulting in the appearance of the strongest compression region of the acoustic front near the upper shock interception $(+\varphi_{\text{crit}})$.

$\varphi = -140°, 40°, 10°, 60°, 140°$ from experimental data were substituted into Eq. (5) to determine the coefficients. This led to the result

$$P(\varphi) = 0.0206 \sin 2\varphi - 0.0072 \cos 2\varphi - 0.0045 \sin\varphi - 0.0023 \cos\varphi + 0.0063 \quad (5a)$$

The agreement between the experimental pressure amplitude distribution along the *entire* wave front and that given by Eq. (5a) is very good (Fig. 4).

## Discussion

The agreement between the relative orders of magnitude of pressure amplitude along the circumference of the cylindrical acoustic front, obtained theoretically in previous investigations as well as experimentally in this investigation, is good within most of the first compression region. The actual form of the pressure distribution, however, seems to be best represented by the semiempirical harmonic function given as Eq. (5a), which consists of a superposition of quadrupole, dipole, and simple acoustic source terms. The physical origin of each term may be hypothesized and it is seen that in some instances a counterpart within the theories and/or comments by Ribner as well as Hollingsworth and Richards may be found. Referring to Eq. (5), the first and second terms taken individually represent pure lateral quadrupole sources. The sine quadrupole has axes inclined at 45° to the shock front and is the largest contributing term. The cosine quadrupole has axes inclined at 90° to the shock front. If the cosine term is taken in combination with a portion of the constant term (zero order harmonic), a longitudinal quadrupole aligned either perpendicular or parallel with the shock front arises.

In Lighthill's theory of aerodynamic noise generation, a quadrupole source is seen to arise as the result of the application of a stress couple to fluid elements at rest. This is shown to be equivalent to the actual physical existence of turbulent velocity fluctuations. The abrupt change in vortex particle velocity across the moving shock front may be resolved into time-varying quadrupole components as the shock wave progresses through the vortex flow field. Powell[10] has demonstrated that the acceleration of a vortex filament in a direction normal to its axis generates a dipole far field. In the case of shock-vortex interaction, deceleration of the vortex takes place as the convective speed of the vortex is abruptly reduced to zero by the reflected shock front as mentioned earlier. Additionally, Curle[11] has shown that, in the presence of solid boundaries, dipole and monopole acoustic sources may appear. If the shock front is regarded as a flow boundary, the statically unbalanced pressure force acting in the direction of shock motion varies with time as the shock front traverses different portions of the vortex. This "force source" is in the form of a cosine dipole with the expansion portion trailing the compression portion. This may be responsible, in part, for the existence of a definite expansion region near $\varphi = 0°$.

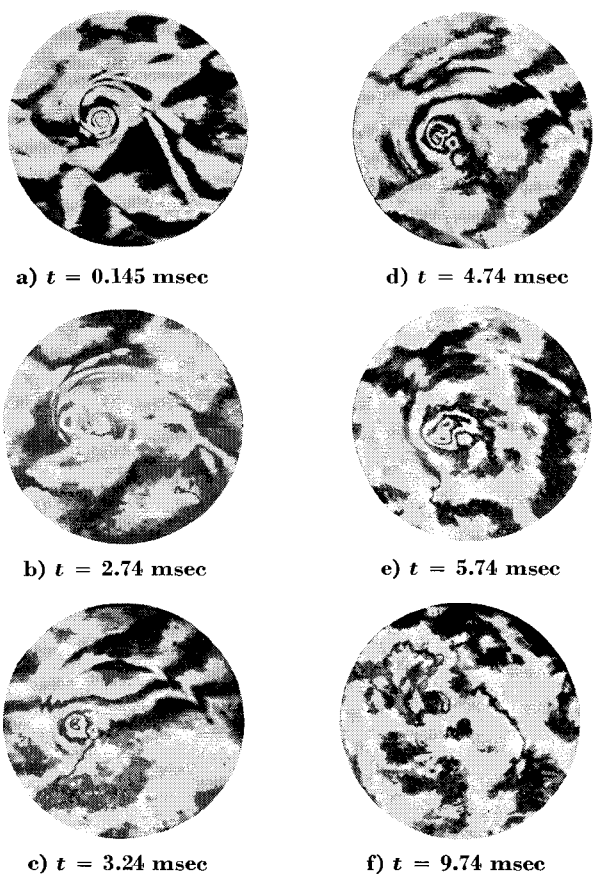


**Fig. 5 Decay sequence of transmitted vortex; infinite fringe interferograms $S = 1.80$ and $\alpha = 12.0°$.**

It was mentioned that the reflected shock is distorted as it passes through the spiral vortex flow field. The upper portion moving with the vortex flow is advanced, whereas the lower portion opposed by the vortex flow is retarded (Fig. 2b). The measured strength of the upper and lower straight portions for the operating conditions corresponding to Fig. 3 was, respectively, $\mp 1\%$ of the reflected shock strength before interaction. It was estimated upon examination of several interactions near $t = t_0$, that the greatest shock front inflection angle observed was about 20° measured from the undisturbed shock front. It is suggested that, because of this shock inflection, a component of the "force source" will be parallel to the undisturbed shock front and this may give rise to a sine dipole whose magnitude could be estimated from the average inclination of the shock front. This would also contribute to the presence of the positive shift of the reversal point near $\varphi = 0°$. This effect was pointed out by Hollingsworth and Richards who detected the presence of a finite value of $P(\varphi = 0)$ in their earlier schlieren data. In a private communication, Ribner suggested that the inflected shock (neglected in his linearized theory) results in a rotation of the coordinate system and, therefore, in a shift of the reversal points. However, this does not explain the fact that none of the shifts at $\varphi = \pm 90°$ and 0° are of equal magnitude.

The most elementary of the terms present in Eq. (5) is, in part, a monopole acoustic source. It was mentioned that any longitudinal quadrupole terms present involve a zeroth-order harmonic and, therefore, the actual numerical value of the constant would also include this component. The physical reason for the appearance of the monopole source was argued by Ribner.[5] He suggested that the vortex is sufficiently strong so that the pressure reduction at the core is substantial. The linearized shock wave-shear interaction theory did not allow for this. He hypothesized that the core pressure just after interaction is in excess of the required equilibrium value of the transmitted vortex and that this excess pressure radiates in the form of a radially symmetric compression wave that coalesces with the wave front generated as a result of the shear wave-shock interaction. The net effect of this compression wave would be to reinforce the compression portions and attenuate the rarefaction portions. Schlieren and interferometric evidence supports this argument (see section on "Vortex Flow Field"). This compression wave alone could possibly account for the $\varphi = \pm 90°$ reversal shifts where the compression regions are extended, but fails to account for the $\varphi = 0°$ shift where the expansion wave is extended. If the linearized theory were to be modified to include the combined effects of the shock inflection that varies with time and the excess pressure radiation, it may account for the observed shifts in the reversal points.

The time behavior (radial decay) of the acoustic wave was examined near $\varphi = -\varphi_{crit}$, i.e., $P(\varphi)_{max}$. Although the maximum pressure amplitude decreases monotonically with

radius, from the preliminary analysis so far it does not appear to entirely follow either the $R^{-1}$ behavior hypothesized by Hollingsworth and Richards (Eq. 1) or the $R^{-1/2}$ behavior predicted by Ribner (Eq. 2). Rather, it appears to be made up of two regions, the first ($R < 10r_{0T}$) behaving as $R^{-1}$ and the second ($R > 10r_{0T}$) more like $R^{-1/2}$.

## Vortex Flow Field

As stated previously, the translational motion of the vortex is halted upon its interaction with the reflected shock front. It is of interest to examine the time behavior of such a vortex in a stationary medium. The vortex flow field was examined for several values of delay time both before and after shock interaction. A sequence of typical interferograms of the transmitted vortex is shown in Fig. 5. It is seen that, within 3 msec, the transmitted vortex has nearly decayed to the vanishing point. Somewhat before this time, however, a secondary high-density region appears, growing steadily in strength. This region is observed to split into a two-celled configuration during its period of growth (Fig. 5d). The high-density region continues to spread in size and strength and vanishes beyond $t = 10$ msec. At about the time of disappearance of the primary vortex, a second vortex appears at a location that is somewhat displaced from the position occupied by the primary vortex. The secondary vortex first grows and then decays during the lifetime of the high-density region. The analysis of a sequence of single fringe interferograms, such as those of Fig. 5, and the corresponding multiple fringe interferograms yielded the spatial density distribution through the center of the vortices and high-density region as illustrated in the inset of Fig. 6. The relative locations of the various flow structures are also shown there to scale corresponding to Fig. 5b. Typical characteristics of the vortex and the associated induced flow-field density distribution are presented in Fig. 6 at three successive stages ($t = 1.5$, 2.5, and 3.5 msec). It is evident that, whereas the primary vortex decays during the first 2.5 msec., the high-density region, originating about a millisecond after interaction, grows in size and strength. At 3.5 msec the primary vortex has disappeared and the secondary vortex is growing. This flow pattern can be reproduced consistently for the time interval $t - t_0 = 10$ msec, beyond which additional secondary vortices appear randomly. This behavior of the flow field is perhaps related to the stability of the slipstreams, which are attached to the spiral vortex. Before shock interaction, these slipstreams seem stable in so far as they appear self-similar over an extended period. However, the slipstreams are refracted by shock interaction,[2] probably tend to become unstable, and within 3 msec after interaction break down into secondary vortex flow. The secondary vortices and the unusual presence of high-density region accompanying the decay of the transmitted vortex were not apparent in the neighborhood of the vortex-before-interaction even when the observation time was extended indefinitely.

The over-all behavior of the vortex decay process after interaction can be conveniently represented in a plot of minimum (core center) density of the vortices and the maximum density in the high density region as a function of time (Fig. 7). The time behavior of the core center density of the vortex-before-interaction is included for comparison. The plot of $\Delta\rho/\rho_2$ is terminated in the figure to avoid confusion. It is apparent that the vortex decays essentially in the same manner both before and after its interaction with the shock front. However its minimum (core center) density decreases abruptly at the instant of interaction. This observation, combined with the observed reduction in core size, suggests that the vortex has been regenerated, i.e., the early stage of its lifetime has been extended. The final stage of the transmitted vortex lifetime, however, has been shortened, most likely because of the presence of the observed secondary concentrated flow regions. The temporal decay behavior of

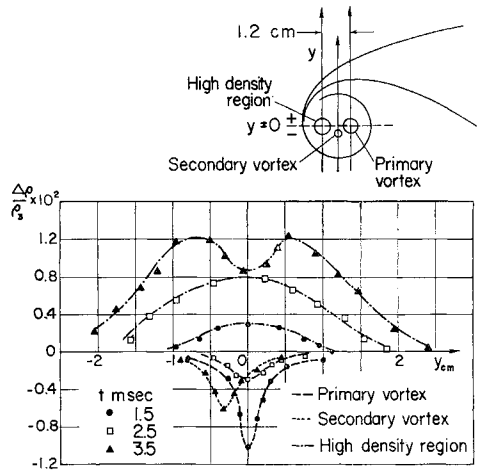


**Fig. 6 Spatial density distribution of transmitted vortex flow field at a few selected times (operating conditions correspond to Fig. 5).**

the primary transmitted vortex can be determined approximately in the following manner. The tangential velocity distribution obtained from analysis of an incompressible viscous circular vortex flow is[12]

$$w = (\Gamma_{0T}/2\pi r)[1 - \exp(-r^2/4\nu\bar{t})] \tag{6}$$

This is a reasonable approximation since the central part of the vortex is nearly circular (see Fig. 2a) and compressibility effects are small (the largest value of density change detected being of the order of 5% of the ambient value). It is further assumed that the vortex is unaffected by interactions with the multiply reflected weak shock system. The viscous, compressible form of the Navier-Stokes equations for radial momentum can be reduced to

$$w^2/r = (1/\rho)(\partial p/\partial r) \tag{7}$$

Assuming a polytropic process in the radial direction, i.e., $p = c\rho^k$, Eqs. (6) and (7) combine to yield

$$\rho^{k-2}\frac{\partial\rho}{\partial r} = \frac{\Gamma_{0T}^2}{4\pi^2 kcr^3}\left(1 - \exp\frac{-r^2}{4\nu\bar{t}}\right)^2 \tag{8}$$

In general $\rho = \rho(r, \bar{t})$, but introducing $r_0 = 2(1.256\nu t)^{1/2}$ obtained by maximizing $w$ (Eq. 6), and letting $r = \eta r_0$ we have for Eq. (8)

$$\rho^{k-2}\frac{d\rho}{d\eta} = \frac{\Gamma_{0T}^2}{16\pi^2 kc(1.256\nu)} \times \frac{1}{\eta^3\bar{t}}[1 - \exp(-1.256\eta^2)]^2$$

where now $\rho = \rho(\eta)$ only. The integration is carried out

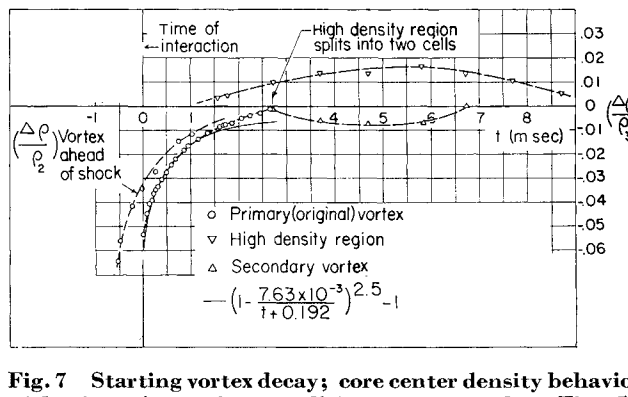


**Fig. 7 Starting vortex decay; core center density behavior with time (operating conditions correspond to Fig. 5).**

from the vortex center to a point $\eta_a$ where the density has essentially the ambient value $\rho_3$. That is,

$$\int_{\rho_0}^{\rho_3} \rho^{k-2}\, d\rho = \frac{\Gamma_{0T}{}^2}{16\pi^2 kc(1.256\nu)} \frac{1}{\bar{t}} \int_0^{\eta_a} \frac{1}{\eta^3} \times [1 - \exp(-1.256\eta^2)]^2 d\eta \quad (9)$$

Partial integration then leads to the expression

$$\frac{\Delta\rho}{\rho_3} = \frac{\rho_0 - \rho_3}{\rho_3} = \left(1 - \frac{K}{\bar{t} + t'}\right)^{1/(k-1)} - 1 \quad (10)$$

where

$$\bar{t} = t + t' \qquad K = \frac{(k-1)}{k\nu} \left(\frac{\Gamma_{0T}}{4\pi}\right)^2 \frac{\rho_3}{p_3} L(\eta_a)$$

and $L(\eta_a)$ = limit of series solution of the integral in Eq. (9).

The additional time $t'$ is included to establish the virtual origin of the transmitted vortex. Equation (10) is plotted in Fig. 6 where $K$, $t'$, and $k$ were deduced from a three point comparison (the points being chosen such that $0.25 < t < 1$ msec). It was found that $k$ was very nearly equal to 1.4. It can be seen that agreement is in general excellent, except 1) near the time of initial interaction ($t_0 = 0$) where, as stated previously, the vortex has elliptical form and where the highest vortex velocities are encountered, increasing compressibility error, and 2) subsequent to the time of appearance of the adjacent high-density region that apparently accelerates the decay of the primary transmitted vortex.

## Traveling Shock-Vortex Street Interaction

A $\frac{1}{4}$-in.-diam cylinder was substituted for the airfoil. The passage of the shock front and associated drift flow over this cylinder generates a turbulent vortex street (Fig. 8a). Typical Reynolds numbers (diameter based) are of the order of $10^5$ with Strouhal number $N_{st} = 0.22$. This street vortex system differs from the ideal Von Karman street because of the gradual increase in lateral and longitudinal spacing as described by Roshko.[13] The reflected shock front interaction with this street is shown in Figs. 8b and 8c. The schlieren and interferogram both reveal that the shock front distorts. Its central portion advances into the wake flow assuming a shape very similar to the expected velocity distribution of the oncoming wake flow. This behavior is similar to that observed in the case of shock-jet flow interaction[14] where the shock front is either locally advanced or retarded depending upon whether the local jet flow aids or opposes the shock motion, respectively.

It is also clearly apparent that, as a result of shock interaction, the vortex street flow rapidly disintegrates into random turbulent wake flow. As each vortex is halted by the shock front, the adjacent upstream vortex catches up reducing the longitudinal spacing. This results in an increased transverse spacing. This "artificially" induced change in the otherwise stable spacing ratio results in the abrupt dissolution of the vortex street.

Within the range of operating conditions used, no well-defined sound emission was observed in the case of shock-vortex street interaction. The strength of the acoustic front generated in shock-vortex interaction depends, of course, upon the shock as well as the vortex strength. A comparison between the shock-starting vortex interaction and the shock-street vortex interaction was made under similar operating conditions (Fig. 8). For an incident shock strength $S = 1.8$ the circulation of the individual street vortex, obtained approximately from the Von Karman ideal street model,[15] was found to be of the order of 20 ft²/sec. For the starting vortex, however, $\Gamma_0 \sim 30$ ft²/sec corresponding to $\alpha \sim 12.5°$. Therefore, for a realistic comparison, the shock-starting vortex interaction was recorded for the same shock strength but with the airfoil angle of attack adjusted to $\alpha = 6.7°$ to provide $\Gamma_0 \sim 20$ ft²/sec. Contrary to the previous observations with $\alpha = 12.5°$, the only detectable sound radiation was observed to extend not more than 5° beyond $-\varphi_{crit}$. This would seem to be a possible reason for the absence of all but a limited field of detectable sound in the case of shock-street vortex interaction. This limited sound field is, in all probability, further obscured by the highly turbulent nature of the wake flow region behind the reflected shock front.

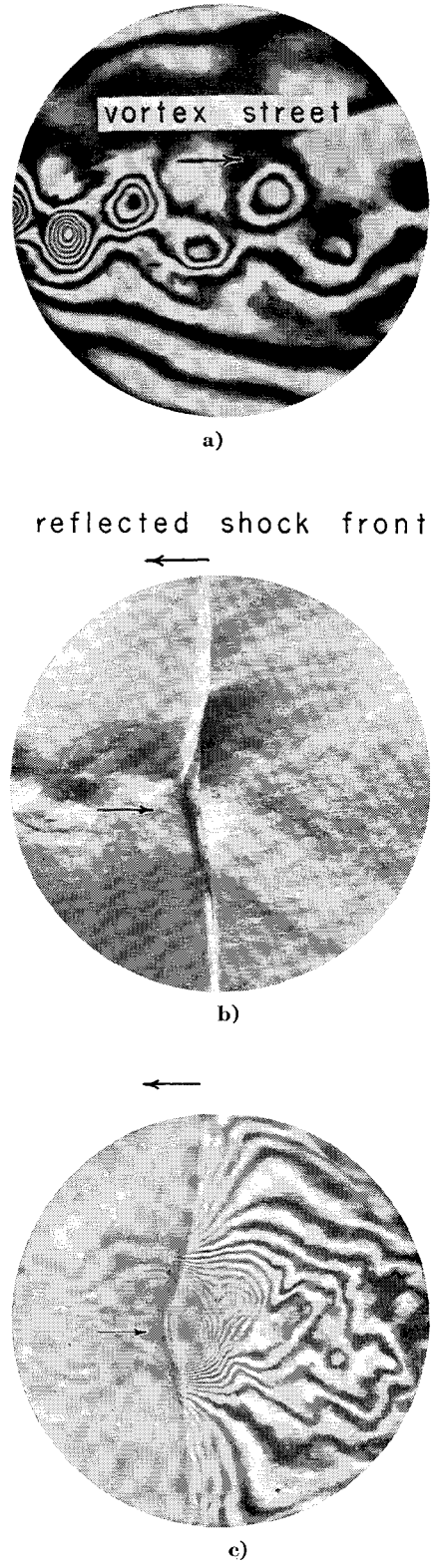


**Fig. 8 Shock-vortex street interaction, $S = 1.91$, $N_{Re} = 1.01 \times 10^5$, cylinder diam = 0.25 in., and $N_{St} = 0.22$.**

## References

[1] Kovasznay, L. S. G., "Turbulence in supersonic flow," J. Aeronaut. Sci. **20**, 657 (1953).

[2] Ribner, H. S., "Convection of a pattern of vorticity through a shock wave," NACA Rept. 1164 (1954).

[3] Hollingsworth, M. A. and Richards, E. J., "A schlieren study of the interaction between a vortex and a shock wave in a shock tube," Aeronautical Research Council Rept. 17985, Fluid Motion Sub-Committee 2323 (1955).

[4] Hollingsworth, M. A. and Richards, E. J., "On the sound generated by the interaction of a vortex and a shock wave," Aeronautical Research Council Rept. 18257, Fluid Motion Sub-Committee 2371 (1956).

[5] Ribner, H. S., "The sound generated by interaction of a single vortex with a shock wave," University of Toronto, Institute of Aerophysics Rept. 61 (1959).

[6] Ruetnik, J. R. and Witmer, E. A., "Transient aerodynamics of two-dimensional airfoils," Part 2, Wright Air Development Center TR 54-368, AD151018 (1958).

[7] Lamb, H., *Hydrodynamics* (Dover Publications, Inc., New York, 1945), 6th ed. Chap. VII, p. 232.

[8] Abbott, I. H., von Doenhott, A. E., and Strivers, L. S., Jr., "Summary of airfoil data," NACA Rept. 824 (1945).

[9] Lighthill, M. J., "Jet noise," AIAA J. **1**, 1507–1517 (1963).

[10] Powell, A., "Theory of vortex sound," J. Acoust. Soc. Am. **36**, 177–195 (1963).

[11] Curle, N., "The influence of solid boundaries upon aerodynamic sound," Proc. Roy. Soc. (London) **A231**, 505–514 (1955).

[12] Lamb, H., *Hydrodynamics* (Dover Publications, Inc., New York, 1945) 6th ed. Chap XI, p. 592.

[13] Roshko, A., "On the development of turbulent wakes from vortex streets," NACA TN 2913, pp. 42–43 (1953).

[14] Weeks, T. M. and Dosanjh, D. S., "Interaction between an advancing shock wave and opposing jet flow," AIAA J. **1**, 1527–1533 (1963).

[15] Birkhoff, G. and Zarantonello, E. H., "Jets, wakes, and cavities," *Applied Mathematics and Mechanics No. 2* (Academic Press Inc., New York, 1957), Chap. XIII, pp. 282–283.


FEBRUARY 1965 AIAA JOURNAL VOL. 3, NO. 2

# A New Technique for the Numerical Analysis of Nonequilibrium Flows

GINO MORETTI*
*General Applied Science Laboratories Inc., Westbury, N. Y.*

**A new technique for the computation of inviscid flows with finite rate chemistry is presented. The case of hydrogen-air combustion is studied in full detail, but this technique can be applied to other mixtures. Difficulties because of instability in existing techniques are eliminated. Consequently, the stepsize in the numerical finite-difference procedure can be increased by 2 to 5 orders of magnitude; the stepsize is unlimited in a state of equilibrium or near to equilibrium. Lengthy calculations that make the programming of two-dimensional flows with finite rate chemistry uneconomical are reduced to a few seconds on a high-speed computer. A comparison of results of this technique with those of other techniques is presented.**

## I. Introduction

IN recent years, several attempts have been made to analyze gaseous flow fields in which the gas is not in chemical equilibrium. Typical problems are nozzle flows,[1–4] wake flows,[5] and stream-tube combustion processes.[6, 7]

In flow problems where the gas may be considered in chemical and thermodynamic equilibrium at every point, two thermodynamic parameters (i.e., the pressure $p$ and the enthalpy $h$) are sufficient to determine any other thermodynamic quantity, either by assuming that the gas is perfect, or by using a fit for the Mollier chart of the gas.

If the gas is not in chemical equilibrium, a point-by-point evaluation of its composition is necessary. Starting at a point on a streamline where all the parameters are known, the mass-fractions $\alpha_i$, the temperature $T$, and the density $\rho$ at the next point are to be determined as functions of $p$, $h$, and the flow time $\Delta t$, elapsed between the two points, taking into account the chemical reactions that occur in the time $\Delta t$. Several species are created and destroyed in the process. The rates of production of all the species at a point may be determined as functions of the macroscopic thermodynamic parameters and the initial composition.

Received February 11, 1964. This work was supported by the Aeronautical Systems Division, Air Propulsion Laboratory, under technical direction of Weldon Worth, under Contract No. AF 33-657-10463.

* Scientific Supervisor. Associate Fellow Member AIAA.

## II. Difficulties of the Numerical Integration

The problem, as stated previously, has no conceptual difficulties. The analysis along a streamline may be performed, in principle, by solving a system of ordinary differential equations with $T$, $\rho$, and the mass fractions as unknowns. Different techniques have been used, including sophisticated schemes such as the Runge-Kutta or the predictor-corrector methods.[7, 8]

Unfortunately, the maximum stepsize $\Delta t$ is severely limited by stability criteria, although the resulting curves of mass fractions vs time are very smooth, when properly computed. Consider, for example, a semilogarithmic plot of the atomic hydrogen mass fraction vs time in a one-dimensional problem of combustion at constant pressure (Fig. 1).[7] In the first phase of the phenomenon ($0 < t < 7 \times 10^{-6}$ sec), the curve is a straight line. The same is true for all the other mass fractions. Moreover, in this range, density, and temperature are constant. Since all the significant parameters are linear functions of time, one could expect correct results from a single-step computation, with a stepsize of the order of $5 \times 10^{-6}$ sec. However, it has been found[7] that steps slightly larger than $1.7 \times 10^{-8}$ sec lead to unstable results. The analysis of processes near equilibrium yields the same